Self-consistent molecular dynamics calculation of diffusion in higher n-alkanes

Nikolay D. Kondratyuk, Genri E. Norman, and Vladimir V. Stegailov

Citation: The Journal of Chemical Physics **145**, 204504 (2016); doi: 10.1063/1.4967873
View online: http://dx.doi.org/10.1063/1.4967873
View Table of Contents: http://scitation.aip.org/content/aip/journal/jcp/145/20?ver=pdfcov
Published by the AIP Publishing

Self-consistent molecular dynamics calculation of diffusion in higher *n*-alkanes

Nikolay D. Kondratyuk,[1,2,a)] Genri E. Norman,[1] and Vladimir V. Stegailov[1]
[1]*Joint Institute for High Temperatures of the Russian Academy of Sciences, Moscow 125412, Russia*
[2]*Moscow Institute of Physics and Technology, Dolgoprudny 141700, Russia*

(Received 12 September 2016; accepted 2 November 2016; published online 23 November 2016)

Diffusion is one of the key subjects of molecular modeling and simulation studies. However, there is an unresolved lack of consistency between Einstein-Smoluchowski (E-S) and Green-Kubo (G-K) methods for diffusion coefficient calculations in systems of complex molecules. In this paper, we analyze this problem for the case of liquid *n*-triacontane. The non-conventional long-time tails of the velocity autocorrelation function (VACF) are found for this system. Temperature dependence of the VACF tail decay exponent is defined. The proper inclusion of the long-time tail contributions to the diffusion coefficient calculation results in the consistency between G-K and E-S methods. Having considered the major factors influencing the precision of the diffusion rate calculations in comparison with experimental data (system size effects and force field parameters), we point to hydrogen nuclear quantum effects as, presumably, the last obstacle to fully consistent *n*-alkane description. *Published by AIP Publishing.* [http://dx.doi.org/10.1063/1.4967873]

I. INTRODUCTION

Decades of molecular modeling and simulation history have not still provided the desirable accuracy of material property calculations in many cases. Diffusion rate calculations in liquids of complex molecules are among them.

There are two equivalent approaches for the calculation of the diffusion coefficient: the Einstein-Smoluchowski (E-S) and Green-Kubo (G-K) methods.[1] The first one uses a mean-square displacement (MSD), the second takes an integral of a velocity autocorrelation function (VACF). The E-S formula is used more frequently in molecular dynamics (MD) simulations[2–30] than the G-K method[2,7,11,13,14,17,29,30] because MSD is easier to interpret and due to the problems with integration to infinite time in the G-K method. The agreement between both methods is demonstrated in the case of atomic and simple molecular liquids.[11,14,29] The disagreement appears in polyatomic molecular systems: the G-K method gives overestimated values in comparison with the E-S approach.[2,7,13,17] The reason for this discrepancy has not been understood yet.

The first simulation results on diffusion were obtained for *n*-butane liquid.[2] The united-atom approach was used with frozen bond and angle values. The rotation of the end atoms around the central bond (dihedral interaction) was adjusted to the experimental data that were available at that moment. The authors used both E-S and G-K methods and the G-K method gave the overestimated values of diffusivity. The more complicated form of the united-atom force field was used for understanding the nature of diffusion in *n*-pentane and *n*-decane.[3,4] Padilla and Toxvaerd showed (by varying CH_X-CH_2-CH_2-CH_X torsion barriers) that the diffusion in *n*-alkanes depends on the dihedral interactions and hypothesized that molecular flexibility determines the decay of VACF. Lee and Pak[7] showed the agreement of both the methods for some *n*-alkanes up to *n*-$C_{17}H_{36}$ but the asymptotic behavior of VACF was not studied also.

Later, molecular dynamics studies of the thermodynamic properties and the calculations of diffusivity using the E-S relation for various alkanes were published: for *n*-decane, *n*-tetracosane, and squalane,[5] for branched alkanes,[6] for *n*-alkanes ($6 \le n \le 66$),[8] for *n*-$C_{100}H_{202}$,[31] for C_{30} isomers,[9] for *n*-dodecane,[18] for hexane, decane, and heptadecane,[32] and for polyethylene.[33] The united-atom force fields were used in most of these works and were shown to overestimate diffusion coefficients. The VACF asymptotes have not been studied enough for systems of complex molecules (*n*-alkanes in particular).

The long-time tail of VACF reflects the physical nature of the system. It decays exponentially in Brownian gases. VACF has two asymptotic exponential regimes in nanoparticle liquids.[10,12,15] The oscillation behavior of VACF is obtained for an ion movement in a liquid.[34] A hydrodynamic power law $t^{-3/2}$ is predicted in the case of atomic liquids and dense gases.[35] It is a result of collective motions. Simulations for Lennard-Jones liquids demonstrate this fact.[12,36–40]

Here, we use *n*-triacontane (*n*-$C_{30}H_{62}$) as an example of a polyatomic molecule. In Section II, we describe the force fields, simulation details of MD, and the equilibration process. The E-S method is considered in Section III: the averaging technique, the results obtained, and system size effects. The G-K method is treated in Section IV: the averaging technique, VACFs, their asymptotes, and the numerical integration problem. The convergence between the E-S and G-K methods is achieved in Section V. The diffusion coefficients obtained are compared with experimental data at different temperatures in Section VI.

a)Email: kondratyuk@phystech.edu

II. MODELING AND SIMULATION TECHNIQUES

A. Force fields for *n*-triacontane

The potential energy of the *n*-triacontane liquid can be modeled as follows:

$$E = \sum_{bonds} K_{bond}(\mathbf{r} - \mathbf{r}_{eq})^2 + \sum_{angles} K_{angle}(\theta - \theta_{eq})^2 + \sum_{dihedrals} \sum_{i=1}^{4} K_i(1 + (-1)^{i+1} \cos i\phi) + \sum_{i=1}^{N-1} \sum_{j>1}^{N} \left\{ 4\epsilon \left[(\sigma/r_{ij})^{12} - (\sigma/r_{ij})^6 \right] + Cq_iq_j/r_{ij} \right\},$$

where the first three terms are valence bond, valence angle, and dihedral interactions correspondingly. Non-bonded forces are described by Lennard-Jones and Coulomb terms.

Two all-atom force fieldsare used: Optimized Potentials for Liquid Simulations All-Atom (OPLS-AA)[41] and its modified version for long hydrocarbonsL-OPLS-AA.[42] The simulation with the Transferable Potentials for Phase Equilibria United-Atom (TraPPE-UA)[43] potential is performed at 353 K, 400 K, and 450 K to show effects connected with the absence of hydrogen atoms in the model.[5,6,8,9,44–46]

B. Details of molecular dynamics calculations

All the diffusivity calculations in the all-atom models are performed for the equilibrated systems of the 3375 $C_{30}H_{62}$ molecules. In the case of TraPPE-UA, the system size is 8000 molecules. Non-bonded 1-4 interactions are scaled with 0.5 factor in the OPLS-AA and the L-OPLS-AA simulations. The cutoff radius is 12 Å in the all-atom force fields and 14 Å in the TraPPE-UA potential. Long-range Coulomb interactions are calculated using the particle-particle particle-mash method.[47]

The NVE ensemble[48] is used. The equations of motion are integrated with a timestep of 1 fs. The simulations are performed in periodic boundary conditions (PBCs) using the LAMMPS package.[49]

C. System equilibration

The equilibration procedure is done in the following way. The initial configuration is gas of the 125 replicated *n*-triacontane molecules. The distance between them is larger than the force field cutoff radius. At the first stage, the temperature is set to 600 K. This temperature is needed to disorder the initial structure rapidly. After 0.1 ns of the NVE integration, the molecules get random orientations. The second stage is the compression to the experimental density 0.77 g/cm^3 for 0.1 ns. The third stage is the relaxation in the NPT ensemble for 2 ns (P = 1 atm, T = 360 K). The average density at the last 0.5 ns is chosen as the equilibrium density for the given force field at 360 K. The fourth stage is the relaxation in the NVT ensemble at the same equilibrium density for 2 ns. The last stage is the relaxation in the NVE ensemble for 0.5 ns after creating the velocity distribution that corresponds to 700 K and cooling back to 360 K in the NVT ensemble. The total linear momentum of the system is zeroed at the end of the relaxation process because the flow (that can be created during the relaxation process) affects the accuracy of the diffusivity calculation.

The relative shape anisotropy parameter κ^2 is used during the relaxation process in addition to the temperature, pressure, and density. This parameter can be found from the following equation: $\kappa^2 = (\lambda_1^4+\lambda_2^4+\lambda_3^4)/(\lambda_1^2 + \lambda_2^2 + \lambda_3^2)^2 - 1/2$, where λ_1, λ_2, and λ_3 are the eigenvalues of the molecule inertia tensor divided by its mass. $\langle\kappa^2\rangle$ reflects the information about the average molecule conformation in the system (for details see Ref. 50).

It is not computationally efficient to repeat this equilibrating process for each other temperature; thus, the following technique is used. Each subsequent temperature and density state is obtained from the previous one. The first stage is creating the velocity distribution that corresponds to 700 K. The system is compressed to the Yaws[52] fit density in the NVE ensemble for 100 ps at the second stage. The third stage is relaxation in the NVT ensemble at the desired T value. At the fourth stage, the system relaxes in the NPT ensemble ($P \sim 1$ atm) for 500 ps and the average density is calculated during this stage. The fifth stage is compressing from the end instantaneous density to the average density in the NVE ensemble for 100 ps. After all, the total system linear moment is zeroed, and the velocity distribution is scaled to the value of T.

The calculations of the *n*-triacontane diffusivity are performed for the obtained densities and temperatures that are shown in Fig. 1. OPLS-AA (the blue open circles) reproduces the densities which correspond to the experimental values from the Tataevsky's book[51] (the dashed red curve with triangles). L-OPLS-AA (the green circles) underestimates the density systematically by 2%-3% in comparison with the experimental data. The TraPPE-UA force field (the dark red circles) gives the densities that are close to the Yaws[52] equation of state (the black dashed curve). The calculations in L-OPLS-AA and TraPPE-UA for the experimental density at 400 K are performed to evaluate the influence of density on the diffusion coefficient. Such a sophisticated relaxation procedure with

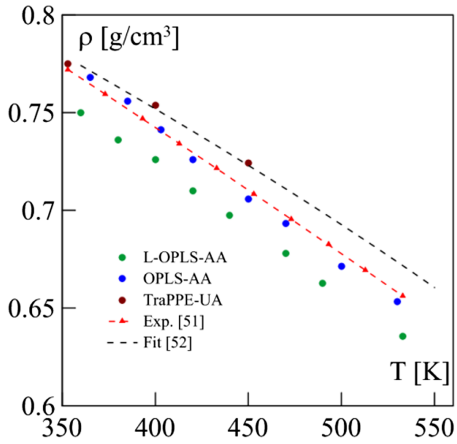

FIG. 1. The equation of state for *n*-triacontane at P = 1 atm (density ρ vs. temperature T). The circles are the equilibrium densities obtained in the L-OPLS-AA (green filled), the OPLS-AA (blue open), and the TraPPE-UA (dark red filled) force fields after the relaxation process. The dashed red curve with triangles corresponds to the experimental data,[51] the black dashed line is the Yaws equation of state.[52]

respect to monoatomic liquids is connected with the complex structure of the *n*-triacontane molecule.

III. EINSTEIN-SMOLUCHOWSKI METHOD

The self-diffusion coefficient D can be obtained from the long-time limit of the molecular center of mass (COM) MSD $\langle \Delta \mathbf{r}^2 \rangle$ using the E-S relation $\langle \Delta \mathbf{r}^2 \rangle = 6Dt + const$.

A. Averaging technique

The diffusivity simulation is performed for the systems of 3375 (OPLS-AA, L-OPLS-AA) and 8000 (TraPPE-UA) molecules in the NVE ensemble. These configurations are obtained by replicating the equilibrated systems of 125 molecules. The initially identical parts of the replicated systems become statistically independent at the time scale of picoseconds. This time is significantly less than full MD trajectories. The averages for MSDs and VACFs are obtained from 1 ns equilibrated MD trajectories. The following technique is used.

The whole trajectory is divided into statistically independent parts. At the first step $\tau_0 = 0$, the average is taken over the molecules

$$\langle \Delta \mathbf{r}^2 \rangle_{\tau_0}(t) = \sum_{i=1}^{N} (\mathbf{r}_i(t + \tau_0) - \mathbf{r}_i(\tau_0))^2 / N, \quad (1)$$

where N is the number of molecules. The second step is the additional averaging over the intervals that is achieved by the shifting of the time point τ_i,

$$\langle \Delta \mathbf{r}^2 \rangle(t) = \sum_{i=1}^{M} \langle \Delta \mathbf{r}^2 \rangle_{\tau_i}(t) / M, \quad (2)$$

where M is the number of independent moments τ_i.

The duration of these shifting intervals should be more than the value of the dynamic memory time t_{mem}.[48] This time corresponds to the moment when the numerical solution of the equations of motion forgets its initial conditions due to the Lyapunov instability. The obtained estimates of the dynamic memory time are about 1.5 ps in the all-atom force fields and about 2.5 ps in the TraPPE-UA potential (for more information see Appendix A). The t_{mem} value is higher in the united-atom model due to the absence of hydrogen atoms which oscillate faster than pseudo atoms CH_2 and CH_3.

B. Mean-square displacements

MSD $\langle \Delta \mathbf{r}^2 \rangle(t)$ in such basic systems as Lennard-Jones gases and liquids has two smoothly connected regimes: the ballistic regime $\langle \Delta \mathbf{r}^2 \rangle = v^2 t^2$ and the diffusive regime $\langle \Delta \mathbf{r}^2 \rangle = 6Dt$. Pomeau[36] predicts more general asymptotic equation for MSD at times greater than ballistic: $\langle \Delta \mathbf{r}^2 \rangle(t) \simeq 6Dt + \sum_{n=1}^{\infty} a_n t^{1/2^n} + const$. However, the non-linear terms do not appear in simple liquids due to the predominance of the linear term.

The n-$C_{30}H_{62}$ MSD has a subdiffusive part between the ballistic and diffusive regimes in both all-atom force fields (Figs. 2(a) and 2(b)) where $\langle \Delta \mathbf{r}^2 \rangle \sim t^{\alpha}, \alpha < 1$. The subdiffusion corresponds to the second part of the Pomeau MSD equation and demonstrates the predominance of the non-linear terms at intermediate time scales. The situation when such translational regime appears is studied in many theoretical, numerical, and experimental works.[14,19,21,26,27,29,53,54] The reasons of this regime can be described in the following way. The molecules are entangled and do not have enough energy to escape from the neighbor cages at low temperatures because the system is closely packed. At higher temperatures, the subdiffusive regime is less pronounced because the molecules are able to move more freely due to the increase of the kinetic molecule energy and the decrease of the density.

The diffusion coefficients are obtained from the linear asymptotes of $\langle \Delta \mathbf{r}^2 \rangle(t)$. A test MSD calculation is performed up to 10 ns to show that the linear asymptote stays the same (Fig. 3).

C. System size effects for the Einstein-Smoluchowski method

Yeh and Hummer[55] showed that the system-size correction which appears due to PBC should be applied in the E-S method. It scales as $BN^{-1/3}$, where N is the number of molecules.[55] Yeh and Hummer used 2000 H_2O molecules, and the correction was about 10% of the absolute value of diffusivity. The results of diffusivity calculations for different

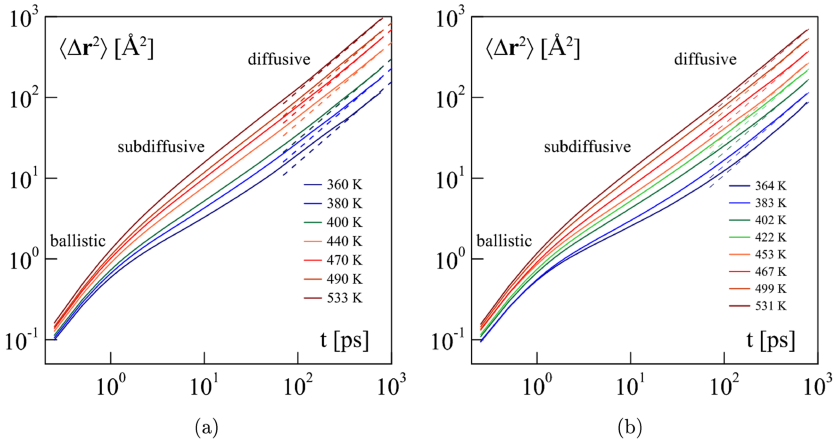

FIG. 2. The MSD time dependence at different temperatures in the L-OPLS-AA (Fig. 2(a)) and OPLS-AA (Fig. 2(b)) force fields. The dashed lines correspond to the linear infinite-time asymptotes.

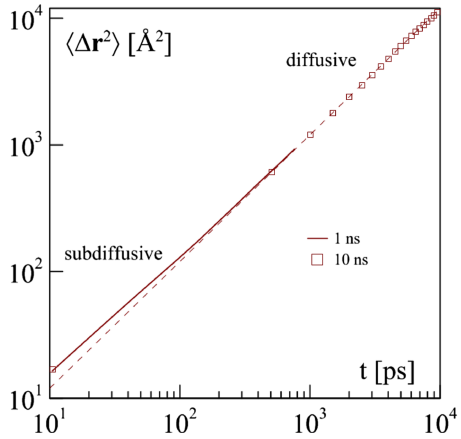

FIG. 3. MSD time dependencies at the larger time scale in the L-OPLS-AA force field at 533 K. The solid curve and dashed line are MSD and linear asymptote, respectively, from Fig. 2(a). Squares correspond to MSD up to 10 ns. The coloring is the same as in Fig. 2(a).

system sizes in L-OPLS-AA at 400 K and TraPPE-UA at 353 K are shown in Fig. 4. The obtained size correction is about 6% for 3375 molecules in the all-atom models and 4% for 8000 molecules in the TraPPE-UA potential. The interesting fact is that the value of B is similar in both models.

The D_{E-S} temperature dependencies match the Arrhenius equation $D_{E-S} = D_0 \exp(-\Delta E/k_B T)$, where ΔE is the effective activation energy and k_B is the Boltzmann constant. The values of D_0 and ΔE for OPLS-AA, L-OPLS-AA, and TraPPE-UA are presented in Table I. The comparison with the experimental values of D is discussed in Section VII.

IV. GREEN-KUBO METHOD

Also, the diffusion coefficient is given by the theoretically equivalent G-K integral formula: $D = \int_0^\infty C_v(t)dt/3$, where $C_v \equiv \langle \mathbf{v}(0)\mathbf{v}(t)\rangle$ is the molecule COM velocity autocorrelation function (VACF), $\mathbf{v}(0)$ and $\mathbf{v}(t)$ are the molecule COM velocities at time moments 0 and t.

A. Averaging technique

The same averaging technique as in Sec. III A is used.

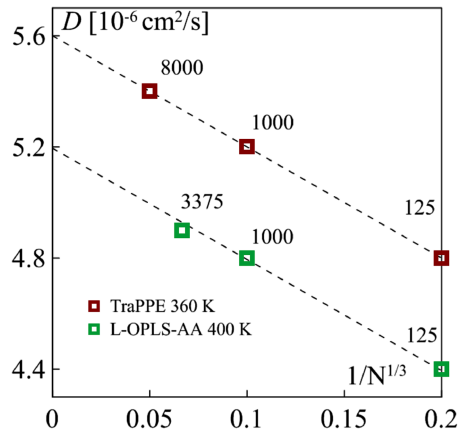

FIG. 4. The dependence of the diffusivity on the size of system in the TraPPE-UA (at 353 K) and L-OPLS-AA (at 400 K) force fields.

TABLE I. The Arrhenius equation parameters D_0 and ΔE obtained using the Einstein-Smoluchowski method in the OPLS-AA, L-OPLS-AA, and TraPPE-UA force fields

Force field	OPLS-AA	L-OPLS-AA	TraPPE-UA
D_0	1700 ± 50	1630 ± 30	730 ± 20
ΔE	4.9 ± 0.2	4.6 ± 0.1	3.5 ± 0.1

$$\langle \mathbf{v}(0)\mathbf{v}(t)\rangle_{\tau_0} = \sum_{i=1}^{N} \mathbf{v}_i(\tau_0)\mathbf{v}_i(t+\tau_0)/N,$$

$$\langle \mathbf{v}(0)\mathbf{v}(t)\rangle = \sum_{i=1}^{M} \langle \mathbf{v}(0)\mathbf{v}(t)\rangle_{\tau_i}/M.$$

The difference between both calculation methods lies in the range of time scales. The characteristic times when the asymptotic tails of the VACF can be obtained (~ 5 ps for the systems used in this work) are a hundred times less than the times that are needed for the observing linear $\langle \Delta \mathbf{r}^2\rangle(t)$ asymptote in the case of the E-S method (~ 750 ps). Consequently, the number of intervals M obtained from the same 1 ns trajectory is about 60 in the E-S method (60 values τ_i separated by 4 ps) and $M = 700$ in the G-K method (700 values τ_i separated by 2 ps because the VACF asymptotes require better sampling).

B. Velocity autocorrelation functions

The molecule COM VACFs are calculated from exactly the same trajectories as the COM MSDs (Figs. 5(a) and 5(b)). The negative region of VACF is typical for atomic liquids and dense gases when rebounding collisions are more frequent than scattering collisions.[56,57] The nature of this region in n-$C_{30}H_{62}$ is due to the molecular bending. This effect becomes weaker with the increase of temperature because the density becomes lower (Fig. 1) and the free volume increases.

C. VACF asymptotes

For simple liquids, VACF has the form[36] $C_v(t) \simeq \sum_{n=1}^{\infty} b_n t^{1/2^n-2}$. The authors[39] demonstrate the crossover of the subleading term $t^{-7/4}$ ($n = 2$) at intermediate time scales to the leading term $t^{-3/2}$ ($n = 1$) in the Lennard-Jones fluid. This term corresponds to the Navier-Stokes hydrodynamics regime and is called the hydrodynamic tail.[35,57,58] The physical nature of this asymptote $t^{-3/2}$ can be explained in the following way. The initial momentum of a particle is shared with its neighbors after microscopic times due to the viscous friction. The diameter of this viscous layer rises as a square root of time. The neighbor layer is spherical in a three-dimensional system and the asymptotic power is 3/2.[58]

The sum of VACF terms $\sum_{n=1}^{\infty} b_n t^{1/2^n-2}$ can be approximated by the effective function $t^{-\beta}$, $\beta = 3/2$ in simple liquids. The different β powers can be discovered due to the slow diffusion process in the liquid considered (Figs. 5(a) and 5(b)). The β dependencies on the inverse temperature in the one and the same time interval are shown in Fig. 6.

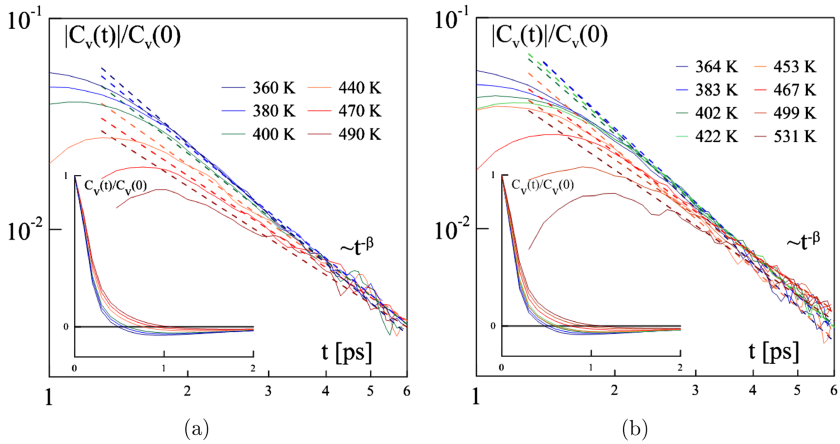

FIG. 5. The asymptotes of the normalized VACF in the L-OPLS-AA (a) and OPLS-AA (b) models at different temperatures. The dashed lines are the VACF tails. Both axes are presented in the logarithmic scale. The coloring is the same as in Figs. 2(a) and 2(b). The full time VACFs are in the left lower corner.

The situation $\beta = 2$ ($n \to \infty$) appears in the OPLS-AA force field (the blue open circles) at low temperatures. β decreases smoothly to the leading term 3/2 as temperature increases and density becomes lower. This β behavior reflects the fact that the dynamics of molecules becomes faster. The hydrodynamic regime ($\beta = 3/2$, $n \to 1$) can be observed at $T > 500$ K which is also confirmed by the absence of the subdiffusion region on the MSD dependence on time.

The shift of the $\beta(1/T)$ dependence to lower temperatures in the L-OPLS-AA force field (the green circles in Fig. 6) could reflect the fact that the melting temperatures of long n-alkanes are lower in L-OPLS-AA than in OPLS-AA.[42] The solidification at the nanosecond time scale in OPLS-AA together with the absence of solidification in L-OPLS-AA is shown in Appendix B.

Note that the values of β in the TraPPE-UA force field (the dark red circles) coincide with the conventional 3/2 hydrodynamic power law and do not depend on the temperature. The non-linear MSD terms are also indistinguishable in our results. Therefore, such unusual values of β in OPLS-AA and L-OPLS-AA can be connected with explicit hydrogen atoms influence in the all-atom force fields.

The VACF tails may be of interest for authors who study the VACF asymptotes in polymers in terms of the mode-coupling approach.[59,60] The results on diffusion are assumed to be a step toward supplementing macroscopic models.[61–64]

D. Numerical integration problem

It is a long-standing question of how to calculate correctly the G-K integral. Some authors considered that it should be cut at t_{PBC}[10,12] for avoiding the influence of PBC. Others suggested to cut VACF when the integral becomes a constant value,[2,7,11,13,14,17,24,29,65] and this technique provides a good agreement between the E-S and G-K methods in simple liquids but not in liquids that consist of complex molecules.[2,7,13,17] Thus, the G-K method gives the overestimated value of the diffusion coefficient in comparison with the E-S method in some n-alkane liquids[2,7] and in ionic liquids[13,17] especially at low temperatures.

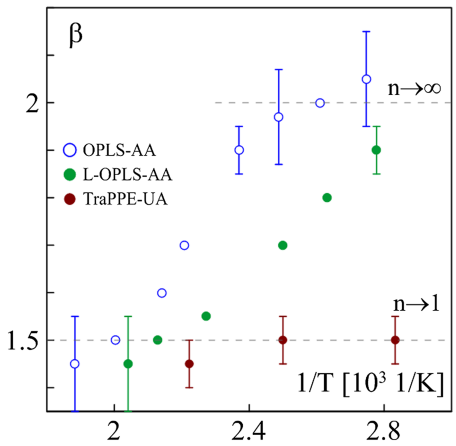

FIG. 6. The circles show β dependencies on $1/T$ for the L-OPLS-AA (green), the OPLS-AA (blue open), and the TraPPE-UA (dark red) force fields. Two gray dashed lines correspond to the first ($n = 1$) and infinite terms ($n \to \infty$) of the Pomeau VACF form.[58]

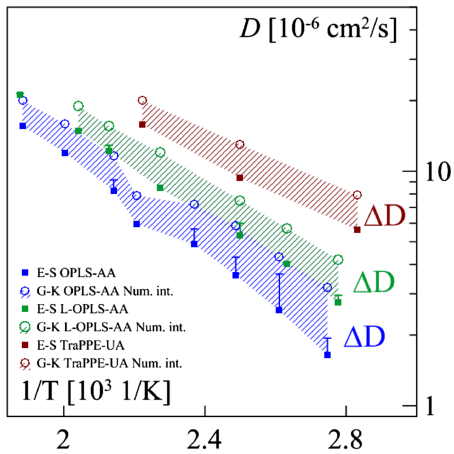

FIG. 7. The values of diffusivity D that are calculated using the Einstein-Smoluchowski (filled squares) and Green-Kubo (open circles) relations in different force fields. The shaded regions show the discrepancies between the theoretically equivalent methods.

The similar problems exist with the calculation of the diffusion coefficient for the *n*-triacontane (Fig. 7). The value of the diffusion coefficient D_{num}^{PBC} that is obtained by the numerical integration of $C_v(t)$ till the moment $t_{PBC} = 7.5$ ps is larger than the E-S value. For example, G-K gives $D_{num}^{PBC} = 18.7 \cdot 10^{-6}$ cm^2/s at $T = 490$ K, but the E-S method gives $14.85 \cdot 10^{-6}$ cm^2/s in the L-OPLS-AA potential.

V. CONVERGENCE OF THE EINSTEIN-SMOLUCHOWSKI AND GREEN-KUBO METHODS

Nichols and Wheeler[30] showed that the VACF integration can be subdivided into the numerical D_{num} and the analytical asymptotic contribution D_a in the binary Lennard-Jones liquid. Such an approach is used to achieve convergence between the E-S and G-K methods in this work as well. The moment when C_v starts to follow $At^{-\beta}$ is about $t_a = 2$ ps (Figs. 5(a) and 2(b)). Thus, at $T = 490$ K in L-OPLS-AA, the numerical part $D_{num} = \int_0^{t_a} C_v(t)dt/3 = 20.9$ cm^2/s and the value of $D_a = \int_{t_a}^{\infty} C_v(t)dt/3 = -5.6 \cdot 10^{-6}$ cm^2/s. The resulting D can be found by summing up these parts of the integral $D = D_{num} + D_a = 15.3 \cdot 10^{-6}$ cm^2/s.

This technique provides the agreement between the E-S and G-K methods at all temperatures (Table II).

We assume that $t^{-3/2}$ can be found at much longer time scales at low temperatures in OPLS-AA and L-OPLS-AA. The problem is that the observation of the VACF terms depends on the system size because of the PBC influence[10,12,37] at times greater than $t_{PBC} \sim L/2v_s$ (where L is the size of the system, v_s is the speed of sound, estimated as 1000 m/s based on the data of Khasanshin and Shchemelev[66]). VACFs for different system sizes in TraPPE-UA are presented in Fig. 8.

We consider that the observation of the hydrodynamic regime $t^{-3/2}$ at low temperatures in the all-atom models is not necessary. The analytical contribution of this term would be several orders of magnitude less at the time scales where $t^{-3/2}$ can be observed.

VI. DIFFERENT FORCE FIELDS VS. EXPERIMENT

Our size-corrected results are compared with the diffusion coefficients measured in the experiment in the wide temperature range[67] (Fig. 9). The error estimation is discussed in Appendix C. The experimental data match the Arrhenius dependence. We see that the OPLS-AA and the L-OPLS-AA force fields predict ΔE quite accurately (4.9 ± 0.2 kcal/mol and 4.6 ± 0.1 kcal/mol, respectively, the experimental value is 4.5 ± 0.1 kcal/mol). The values of diffusion are about 1.8 times lower in the OPLS-AA force field. D_0 coincides with the experimental value in the L-OPLS-AA model at the equilibrium densities of the model (2%-3% lower than the experimental densities). The green area demonstrates the values of D that can be obtained by varying the density back up to the experimental values. It shows that the increase of D_0 in L-OPLS-AA is not just the effect of the higher equilibrium density but also the effect of the change of the force field parameterization.

Conversely to all-atom models, the calculations in the TraPPE-UA model show that the united-atom approach overestimates the diffusion coefficient of *n*-triacontane because the absence of hydrogen atoms increases the molecule free volume. The value of activation energy ΔE is 3.5 ± 0.1 kcal/mol which is much lower than the experimental value. The sensitivity to density variation is higher for TraPPE-UA

TABLE II. The numerical VACF integrals D_{num}, the analytical contributions Da, the resulting D_{G-K} (Green-Kubo), D_{E-S} (size-corrected Einstein-Smoluchowski), and the powers β obtained in the L-OPLS-AA force field

T	D_{num}	D_a	D_{G-K}	D_{E-S}	β
360	6.9	−4.1	2.8	2.75	1.90
380	8.7	−4.9	3.8	4.00	1.80
400	10.5	−5.2	5.3	5.30	1.70
440	15.2	−6.5	8.7	8.50	1.55
470	17.7	−5.8	11.9	12.20	1.50
490	20.9	−5.6	15.3	14.85	1.45

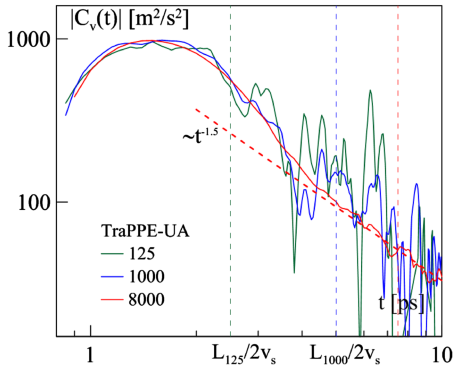

FIG. 8. The dependence of VACF on the size of the system in the TraPPE-UA force field at 353 K. The green, blue, and red curves are VACFs obtained for $N = 125$, 1000, 8000 molecules correspondingly. The dashed vertical lines correspond to the times $LN/2v_s$ (LN is the size of simulation box, v_s is the velocity of sound) when the periodic boundary conditions begin to influence. The red dashed line corresponds to the hydrodynamic tail $At^{-3/2}$.

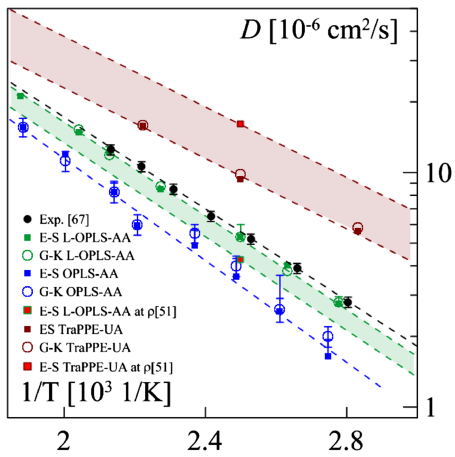

FIG. 9. The comparison of the *n*-triacontane diffusivity D obtained by the E-S (the filled squares) and G-K (the open circles) methods at different T with the experimental data (the black circles)[67] in Arrhenius coordinates for the OPLS-AA (blue), the L-OPLS-AA (green), and the TraPPE-UA (dark red) force fields. The red filled squares are the calculations in the L-OPLS-AA and TraPPE-UA potentials at the experimental density.[51] The filled green areas correspond to the values of diffusion coefficients that can be obtained by varying density from the equilibrium up to the experimental values[51] in the L-OPLS-AA (green) and the TraPPE-UA (dark red) models.

than in the L-OPLS-AA model (see two red filled squares in Fig. 9).

VII. CONCLUSIONS

The MD diffusivity for the *n*-triacontane liquid is calculated using the Einstein-Smoluchowski and Green-Kubo methods. The simulations are performed in the OPLS-AA, the L-OPLS-AA, and the TraPPE-UA force fields at different temperatures.

- The molecule MSDs and VACFs are calculated from the equilibrated MD trajectories. MSDs have pronounced subdiffusive regime in the all-atom force fields at low temperatures. VACF asymptotes $t^{-\beta}$ differ from the conventional hydrodynamic power law $t^{-3/2}$ in this case. These facts validate the thesis that the molecular dynamics is slower in the all-atom force fields than in the united-atom model where both MSDs and VACFs correspond to simple liquids.
- The non-hydrodynamic VACF asymptotic tails in OPLS-AA and L-OPLS-AA are consequences of difficulties in the molecular motion. The subleading terms ($n \geq 2$) of the Pomeau equation $\sum_{n=1}^{\infty} t^{1/2^n-2}$ prevail the hydrodynamic tail $t^{-3/2}$ at low temperatures. The leading term $t^{-3/2}$ starts dominating at 500 K in OPLS-AA and at 470 K in L-OPLS-AA which correspond to the almost not pronounced MSD subdiffusive regimes at these temperatures. On the other hand, the hydrodynamic asymptote occurs in TraPPE-UA at all temperatures considered. It can be connected with the absence of the hydrogen atoms in the model.
- The consideration of the asymptotic tail contribution to the VACF integral is the key to the proper convergence of the diffusivity values obtained by the Einstein-Smoluchowski and Green-Kubo methods. After the careful analysis of the VACF long-time tails and the system size effects, the E-S and G-K methods have been shown to give the same values of the diffusion coefficient. The observation of the hydrodynamic regime $t^{-3/2}$ is not necessary at low temperatures in the all-atom models because of the relatively small analytical contribution of this term to the G-K integral in this case.
- The calculated diffusion coefficients are compared with the experimental data. Both OPLS-AA and L-OPLS-AA force fields reproduce the Arrhenius barrier ΔE with a good accuracy, but the D_0 prefactors are different. On the other hand, TraPPE-UA significantly overestimates the value of diffusivity. Two best force fields for *n*-triacontane considered show a duality: either we have the correct density of liquid *n*-triacontane in OPLS-AA but this liquid is unstable and solidifies with 1.8 times slower diffusion rate or we have the correct diffusion rate and stable liquid but at 2%-3% lower density in L-OPLS-AA. We can suggest a hypothesis that, perhaps, the only way to get a fully consistent description both for the equation of state and for the transport properties of higher *n*-alkanes is to take into account the quantum nature of hydrogen atoms dynamics. Path-integral MD calculations showed that such quantum corrections significantly influence the diffusion in water (see Spura *et al.*[68]). The same effect can be expected for alkanes since the energy of C–H bonds in alkanes is only 20% lower than the energy of the O–H bond in water. The application of the path-integral MD for higher alkanes is too computationally expensive nowadays but might become possible in the near future.

ACKNOWLEDGMENTS

We are grateful to Yong Zhang for his useful comments concerning the size effects and to Roman Ryltsev and Nikolay Chtchelkachov for their helpful comment about the VACF asymptotic terms. We also want to thank Jeffery Klauda, Edward Maginn, and Valery Rudyak for stimulating questions.

The calculations are performed on the MVS-10P cluster of the Joint Supercomputer Center of RAS, the prototype computing cluster "Angara-C1" in JSC NICEVT, and the computing cluster in MIPT. The work is supported by the Russian Science Foundation Grant No. 14-19-01295.

APPENDIX A: DYNAMIC MEMORY TIME

The dynamic memory time can be characterized by the following equations:

$$\langle \Delta \mathbf{r}^2 \rangle = \frac{1}{N} \sum_{i=1}^{N} (\mathbf{r}_i(t) - \mathbf{r}'_i(t))^2, \langle \Delta \mathbf{v}^2 \rangle = \frac{1}{N} \sum_{i=1}^{N} (\mathbf{v}_i(t) - \mathbf{v}'(t))^2, \tag{A1}$$

where $(\mathbf{r}; \mathbf{v})(t)$ and $(\mathbf{r}'; \mathbf{v}')(t)$ are the trajectories with the same initial conditions, integrated using time steps Δt and $\Delta t'$. The asymptotes of these divergences are $\langle \Delta \mathbf{r}^2 \rangle = A \exp(Kt)$ and $\langle \Delta \mathbf{v}^2 \rangle = B \exp(Kt)$, if $t \lesssim t_{\text{mem}}$. $\langle \Delta \mathbf{r}^2 \rangle = 2D(t - t_m)$ and $\langle \Delta \mathbf{v}^2 \rangle = 2\mathbf{v}_{\text{th}}{}^2$, if $t \gtrsim t_{\text{mem}}$, where D is the diffusion coefficient, $\mathbf{v}_{\text{th}} = \sqrt{3k_BT/m}$.

The divergences (3) are calculated for molecule centers of mass using two trajectories integrated with $\Delta t = 0.1$ fs

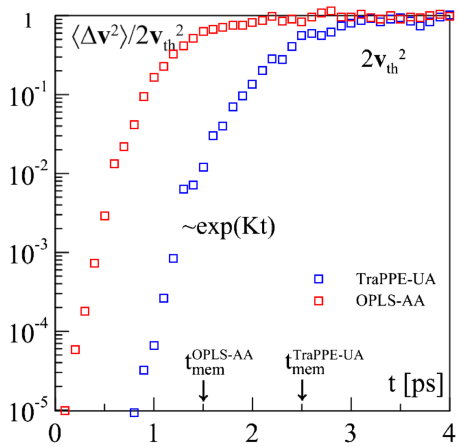

FIG. 10. The dependence of the $\langle \Delta \mathbf{v}^2 \rangle$ on time in the OPLS-AA (the red squares) and TraPPE-UA (the blue squares) force fields. The value of t_{mem} is higher in the TraPPE-UA model due to the absence of hydrogen atoms.

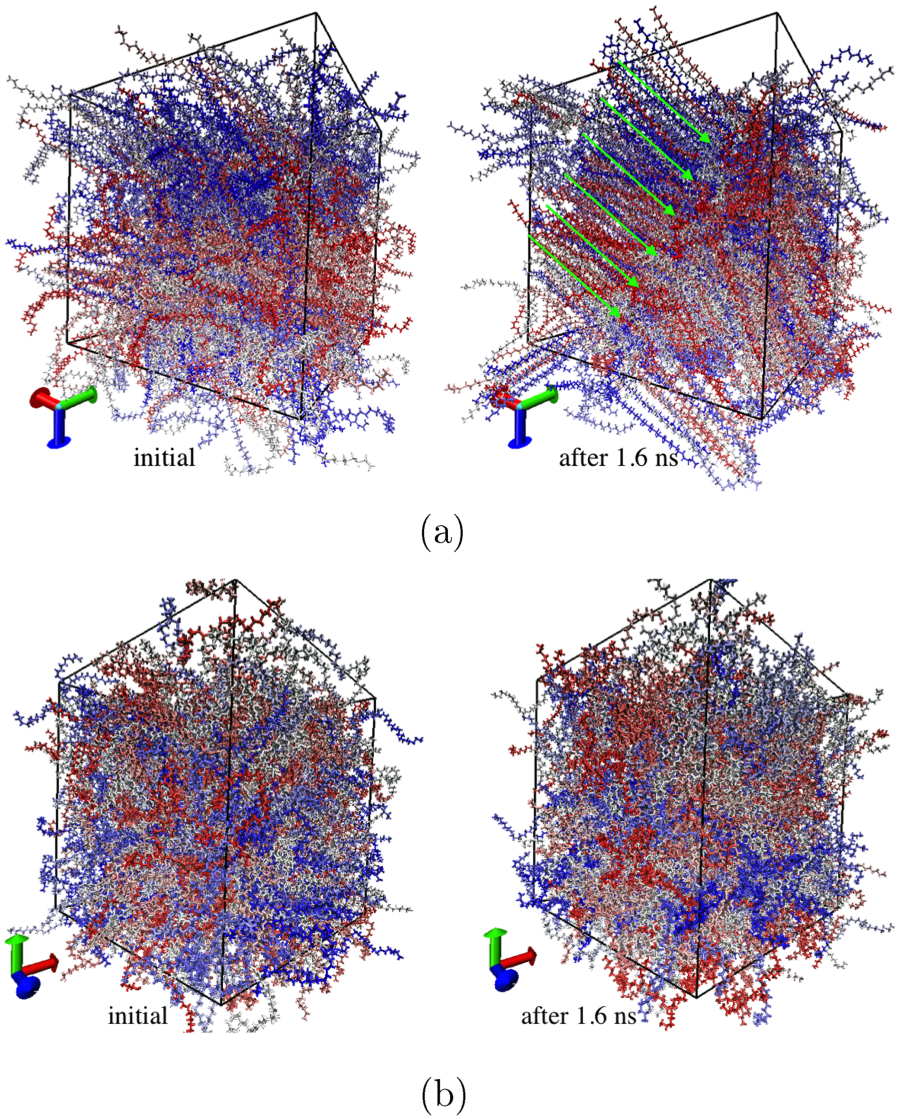

FIG. 11. The initial liquid configurations (N_{mol} = 1000) in the OPLS-AA and L-OPLS-AA force fields at 400 K are shown in the left parts of Figs. 11(a) and 11(b), respectively. The molecules are colored differently to emphasize ordering. The systems after 1.6 ns are presented in the right parts of Figs. 11(a) and 11(b). The green arrows show the domains where the molecules are oriented in one direction.

and Δt = 1 fs (Fig. 10). The obtained estimates of the dynamic memory time are about 1.5 ps in the all-atom force fields and about 2.5 ps in the TraPPE-UA potential.

APPENDIX B: LIQUID-GEL TRANSITION IN OPLS-AA

The errors in OPLS-AA could reflect the fact that the system is not in an equilibrium state. It is a metastable liquid at P = 1 atm and T = 400 K in the OPLS-AA force field which solidifies at the nanosecond time scale (e.g., after about 1.6 ns for the system of 1000 molecules, see Fig. 11(a)). The VMD package[69] is used to visualize the system configurations. The corresponding snapshots of the n-triacontane are presented in Fig. 11(a) (green arrows correspond to the domains where the molecules are oriented in the same direction). Siu *et al.*[42] obtained the same behavior for n-pentane liquid. The modified L-OPLS-AA reproduces liquid n-triacontane (Fig. 11(b)) with no crystal-like domains after 1.6 ns.

APPENDIX C: ERRORS ESTIMATION

1. E-S method

The MSD values are averaged over the X, Y, and Z directions. The errors are the deviations between the average and the maximum value of the diffusivity in a certain direction.

2. G-K method

The error bars of D_{GK} which are pointed in Fig. 9 are determined by the accuracy of β. They are evaluated in the following way. The maximum D_a^{max} (that corresponds to the minimum suitable β) and minimum D_a^{min} (maximum β) analytical integrals are calculated. The average contributions $D_a^{ave} = (D_a^{min} + D_a^{max})/2$ are used to calculate the G-K integrals $D_{G-K}^{ave} = D_{num} + D_a^{ave}$. The errors are the differences between the average and the extreme values of the analytical integrals.

[1]E. Helfand, Phys. Rev. **119**, 1 (1960).
[2]J. P. Ryckaert and A. Bellemans, Chem. Phys. Lett. **30**, 123 (1975).
[3]P. Padilla and S. Toxvaerd, J. Chem. Phys. **94**, 5650 (1991).

[4]P. Padilla and S. Toxvaerd, J. Chem. Phys. **95**, 509 (1991).
[5]M. Mondello and G. S. Grest, J. Chem. Phys. **103**, 7156 (1995).
[6]M. Mondello, G. S. Grest, A. R. Garcia, and B. G. Silbernagel, J. Chem. Phys. **105**, 5208 (1996).
[7]S. H. Lee, H. Lee, and H. Pak, Bull. Korean Chem. Soc. **18**, 478 (1997), available at http://www.journal.kcsnet.or.kr/main/j_search/j_abstract_view.htm?code=B970510&cpage=1&qpage=j_search&spage=j_search&journal=B&vol=18&no=5&page=&year1=1990&year2=1999&view=10&qpage=j_search&abstract=.
[8]M. Mondello, G. S. Grest, E. B. Webb, and P. Peczak, J. Chem. Phys. **109**, 798 (1998); e-print arXiv:9802022 [physics].
[9]J. D. Moore, S. T. Cui, H. D. Cochran, and P. T. Cummings, J. Chem. Phys. **113**, 8833 (2000).
[10]V. Y. Rudyak, G. V. Kharlamov, and A. A. Belkin, High Temp. **39**, 264 (2001).
[11]S. H. Lee, D. K. Park, and D. B. Kang, Bull. Korean Chem. Soc. **24**, 178 (2003).
[12]V. Rudyak, A. A. Belkin, D. Ivanov, and V. Egorov, High Temp. **46**, 30 (2008).
[13]M. H. Kowsari, S. Alavi, M. Ashrafizaadeh, and B. Najafi, J. Chem. Phys. **129**, 224508 (2008).
[14]I. Gholami, A. Fiege, and A. Zippelius, Phys. Rev. E: Stat., Nonlinear, Soft Matter Phys. **84**, 031305 (2011); e-print arXiv:1106.3239.
[15]V. Y. Rudyak, S. L. Krasnolutskii, and D. A. Ivanov, Microfluid. Nanofluid. **11**, 501 (2011).
[16]Y. Wang, P. R. L. Markwick, C. A. F. De Oliveira, and J. A. McCammon, J. Chem. Theory Comput. **7**, 3199 (2011).
[17]H. Liu, E. Maginn, A. E. Visser, N. J. Bridges, and E. B. Fox, Ind. Eng. Chem. Res. **51**, 7242 (2012).
[18]Z. Rao, S. Wang, and Y. Zhang, Phase Transitions **85**, 400 (2012).
[19]G. Ivanovskis, G. Norman, and D. Usmanova, Dokl. Phys. **57**, 427 (2012).
[20]H. Feng, W. Gao, J. Nie, J. Wang, X. Chen, L. Chen, X. Liu, H.-D. Lüdemann, and Z. Sun, J. Mol. Model. **19**, 73 (2013).
[21]D. Vural, L. Hong, J. C. Smith, and H. R. Glyde, Phys. Rev. E **88**, 052706 (2013).
[22]M. Chen, R. Pendrill, G. Widmalm, J. W. Brady, and J. Wohlert, J. Chem. Theory Comput. **10**, 4465 (2014).
[23]T. K. Zahariev, R. I. Slavchov, A. V. Tadjer, and A. N. Ivanova, J. Comput. Chem. **35**, 776 (2014).
[24]S. P. Singh, C.-C. Huang, E. Westphal, G. Gompper, and R. G. Winkler, J. Chem. Phys. **141**, 084901 (2014).
[25]Y. D. Fomin, V. N. Ryzhov, and E. N. Tsiok, J. Chem. Phys. **143**, 184702 (2015).
[26]M. V. Tamm, L. I. Nazarov, A. A. Gavrilov, and A. V. Chertovich, Phys. Rev. Lett. **114**, 178102 (2015); e-print arXiv:1404.2558v1.
[27]G. S. Smirnov and V. V. Stegailov, High Temp. **53**, 829 (2015).
[28]J. Sauter and A. Grafmüller, J. Chem. Theory Comput. **11**, 1765 (2015).
[29]M. Śmiechowski, J. Chem. Phys. **143**, 244505 (2015).
[30]J. W. Nichols and D. R. Wheeler, Ind. Eng. Chem. Res. **54**, 12156 (2015).
[31]W. Paul and G. D. Smith, Macromolecules **30**, 7772 (1997).
[32]D. A. Hernandez and H. Domínguez, J. Chem. Phys. **138**, 134702 (2013).
[33]E. A. Zubova, I. A. Strelnikov, N. K. Balabaev, A. V. Savin, M. A. Mazo, and L. I. Manevitch, "Coarse-grained polyethylene: The simplest model for orthorhombic crystal," Polym. Sci., Ser. A (to be published).
[34]A. V. Lankin, G. E. Norman, and M. A. Orekhov, J. Phys.: Conf. Ser. **653**, 012155 (2015).
[35]B. J. Alder and T. E. Wainwright, Phys. Rev. A **1**, 18 (1970); e-print arXiv:1011.1669v3.
[36]Y. Pomeau, Phys. Rev. A **7**, 1134 (1973).
[37]A. McDonough, S. P. Russo, and I. K. Snook, Phys. Rev. E **63**, 026109 (2001).
[38]K. Meier, A. Laesecke, and S. Kabelac, J. Chem. Phys. **121**, 9526 (2004).
[39]R. E. Ryltsev and N. M. Chtchelkatchev, J. Chem. Phys. **141**, 124509 (2014); e-print arXiv:1407.5462.
[40]N. M. Chtchelkatchev and R. E. Ryltsev, JETP Lett. **102**, 732 (2015).
[41]W. L. Jorgensen, D. S. Maxwell, and J. Tirado-Rives, J. Am. Chem. Soc. **118**, 11225 (1996).
[42]S. W. I. Siu, K. Pluhackova, and R. A. Böckmann, J. Chem. Theory Comput. **8**, 1459 (2012).
[43]M. G. Martin and J. I. Siepmann, J. Phys. Chem. B **102**, 2569 (1998).
[44]P. Ungerer, C. Nieto-Draghi, B. Rousseau, G. Ahunbay, and V. Lachet, J. Mol. Liq. **134**, 71 (2007).
[45]X. Periole and S.-J. Marrink, "Biomolecular simulations. The Martini coarse-grained force field," *Methods in Molecular Biology* (Springer, 2012), Vol. 924.
[46]H. I. Ingólfsson, C. A. Lopez, J. J. Uusitalo, D. H. de Jong, S. M. Gopal, X. Periole, and S. J. Marrink, Wiley Interdiscip. Rev.: Comput. Mol. Sci. **4**, 225 (2014).
[47]R. Hockney and J. Eastwood, *Computer Simulation Using Particles* (CRC Press, New York, 1989).
[48]G. E. Norman and V. V. Stegailov, Math. Models Comput. Simul. **5**, 305 (2013).
[49]S. Plimpton, J. Comput. Phys. **117**, 1 (1995).
[50]N. D. Kondratyuk, G. E. Norman, and V. V. Stegailov, Polym. Sci., Ser. A **56**, 825 (2016).
[51]V. Tataevsky, *Physico-Chemical Properties of Individual Hydrocarbons* (in Russian) (Gostoptekhizdat, Moscow, 1960), p. 108.
[52]C. Yaws, *Thermophysical Properties of Chemicals and Hydrocarbons* (William Andrew, NY, USA, 2008), p. 194.
[53]D. S. Banks and C. Fradin, Biophys. J. **89**, 2960 (2005).
[54]R. Metzler, J.-H. Jeon, A. G. Cherstvy, and E. Barkai, Phys. Chem. Chem. Phys. **16**, 24128 (2014).
[55]I. C. Yeh and G. Hummer, J. Phys. Chem. B **108**, 15873 (2004).
[56]J. M. Haile, *Molecular Dynamics Simulation: Elementary Methods* (John Wiley and Sons, Chichester, 1992).
[57]J. P. Boon and S. Yip, *Molecular Hydrodynamics* (Dover Publications, New York, 1992).
[58]Y. Pomeau and P. Résibois, Phys. Rep. **19**, 63 (1975).
[59]J. Farago, H. Meyer, and A. N. Semenov, Phys. Rev. Lett. **107**, 1 (2011).
[60]J. Farago, A. N. Semenov, H. Meyer, J. P. Wittmer, A. Johner, and J. Baschnagel, Phys. Rev. E: Stat., Nonlinear, Soft Matter Phys. **85**, 1 (2012); e-print arXiv:0402594v3 [arXiv:cond-mat].
[61]M. S. Apfelbaum and E. M. Apfelbaum, J. Electrost. **50**, 129 (2001).
[62]Y. Yan, P. Blanco, M. Z. Saghir, and M. M. Bou-Ali, J. Chem. Phys. **129**, 194507 (2008).
[63]J. G. Hwang, F. O'Sullivan, M. Zahn, O. Hjortstam, L. A. A. Pettersson, and R. Liu, in *Annual Report Conference on Electrical Insulation and Dielectric Phenomena*, *CEIDP*, *2008* (IEEE, 2008), p. 361.
[64]M. S. Apfelbaum, Surf. Eng. Appl. Electrochem. **45**, 102 (2009).
[65]S. Viscardy, J. Servantie, and P. Gaspard, J. Chem. Phys. **126**, 184512 (2007); e-print arXiv:0701254 [cond-mat].
[66]T. S. Khasanshin and A. P. Shchemelev, High Temp. **39**, 60 (2001).
[67]T. Vardag, N. Karger, and H.-D. Lüdemann, Ber. Bunsen-Ges. Phys. Chem. **95**, 859 (1991).
[68]T. Spura, C. John, S. Habershon, and T. D. Kühne, Mol. Phys. **113**, 808 (2015).
[69]W. Humphrey, A. Dalke, and K. Schulten, J. Mol. Graphics **14**, 33 (1996).